Quasiclassical Trajectory Study of the Vibrational Quenching of Hydroxyl Radicals through Collision with O Atoms

Raji Viswanathan,*,† Michelle Dolgos,‡,§ and Robert J. Hinde‡

Department of Chemistry, Yeshiva University, New York, New York 10033, and Department of Chemistry, University of Tennessee, Knoxville, Tennessee 37996-1600

Received: October 16, 2006; In Final Form: November 30, 2006

The collisional removal of vibrationally excited OH radicals by O atoms is studied by the quasiclassical trajectory method. To evaluate the effect of different topological features on the scattering processes two different global potential energy surfaces, DMBE IV and TU, are used. Results for reactive, exchange, and inelastic scattering probabilities are reported for central collisions (with zero total angular momentum) with a fixed relative translational energy for vibrational levels of OH ranging from $v = 1$ to $v = 8$. Vibrational state distributions of product molecules are also compared on the two potential energy surfaces. Both surfaces predict higher probabilities for reaction than for exchange or inelastic scattering. The vibrational state distributions of the product diatomic molecules are different on the two surfaces. In particular, the two surfaces give substantially different probabilities for multiquantum OH vibrational relaxation transitions $OH(v) + O \rightarrow OH(v') + O$.

Introduction

In the terrestrial mesosphere (at altitudes of 80−95 km), the highly exothermic reaction of ozone with atomic hydrogen,

$$O_3 + H \rightarrow OH + O_2 \quad (1)$$

produces vibrationally excited hydroxyl radicals, mainly in the $v = 6-9$ states.[1,2] The excited hydroxyl radicals thereby produced (henceforth written OH*) can lose vibrational energy through emission of infrared photons or through collisions with other species. In the mesosphere, N_2, O_2, and O are considered to be the primary collision partners that can deactivate OH* radicals.[3] Knowledge of the collisional relaxation rates of OH* by these collision partners is necessary to determine the role of reaction 1 in the mesospheric energy balance.

Collisional quenching of OH* by N_2 is significant only for OH* radicals in the $v = 8$ state, where there is a near resonance between the OH* and N_2 vibrational frequencies. The N_2 collisional relaxation rates for other OH* vibrational levels were recently measured and found to be very low.[4] Molecular oxygen is a more effective quencher of OH*, and O_2 + OH* collisional relaxation rate constants have been measured for OH* radicals in the vibrational levels $v = 1-9$.[5−7] These rate constants increase substantially as the OH* vibrational quantum number v increases so that O_2 is very effective at quenching highly excited OH* vibrational levels but less so at quenching OH* radicals with only moderate vibrational excitation.

This leaves atomic oxygen as a potentially important collision partner for the collisional relaxation of mesospheric OH* radicals, particularly those OH* radicals in the $v = 1-4$ levels. The collisional removal of OH* by atomic oxygen can proceed via either inelastic or reactive channels:

$$O^1H + O^2 \rightarrow O^1O^2 + H \quad (2a)$$

$$O^1H + O^2 \rightarrow O^2H + O^1 \quad (2b)$$

$$O^1H + O^2 \rightarrow O^1H + O^2 \quad (2c)$$

Reaction 2a is exothermic by about 13.4 kcal/mol and proceeds through a deep well corresponding to the HO_2 hydroperoxy radical.

Experimental measurements of the vibrational-state-specific rates for these processes are scarce. Spencer and Glass reported the room-temperature rate for the reaction of $OH(v = 1) + O$ to be greater than that for $OH(v = 0) + O$ reaction by a factor of 2 to 3.[8] Recently, Khachatrian and Dagdigian[9] have reported the rate for collisional removal of $OH(v = 1)$ by O atoms to be only slightly larger than that for $OH(v = 0)$. The dearth of experimental information about the rates of reactions 2a−2c for higher vibrational states of OH makes it difficult to construct accurate models of the atmospheric heating due to reaction 1. For example, the effective heating rate of reaction 1 could change by as much as 1 K/day if the rate for OH* removal, whether by inelastic or reactive channels, changes by a factor of 2.[3,10,11] Uncertainty in the rates of reactions 2a−2c is therefore one of the most important factors limiting the accuracy of models of mesospheric chemical heating by reaction 1.[3,11]

In order to provide a better understanding of these energy transfer processes, a number of theoretical investigations have also been carried out using at least two different potential energy surfaces. Varandas recently performed an extensive quasiclassical trajectory (QCT) study[12] of reactions 2a−2c using the double many body expansion (DMBE)[13,14] potential energy surface (PES) for the HO_2 system developed by Pastrana et al.[15] The state-specific vibrational quenching rates obtained in this study for OH* + O collisions at $T = 210$ K showed substantial nonmonotonic variation with the initial OH* vibrational quantum number v. As v increased from $v = 1$ to $v = 4$, the quenching rate constants increased from about 2×10^{-11} cm^3/s

* Corresponding author. E-mail: raji@yu.edu.
† Yeshiva University.
‡ University of Tennessee.
§ Current address: Ohio State University.

10.1021/jp0667947 CCC: $37.00
Published on Web 01/18/2007

to about 3×10^{-11} cm^3/s; with further increases in v, however, the quenching rate constants began to decline, once again reaching values of about 2×10^{-11} cm^3/s at $v = 9$. By comparison, a recent model of the mesospheric energy balance[3] assumed that the overall OH* quenching rate for reactions 2a−2c was 2×10^{-10} cm^3/s, independent of v. This would appear to be an oversimplification.

A series of semiempirical DMBE potentials have been developed for this reaction.[15−17] These semiempirical potentials were fit to ab initio data by Melius and Blint.[18] The ab initio calculations on the doublet ground state of HO_2 (X^2A'') used a multiconfiguration self-consistent field (MCSCF) method with Dunning's [4s2p1d/2s1p] Gaussian type basis sets augmented with an additional d function on the O atom and an additional p function on the H atom. The DMBE parameters were chosen to fit the 406 ab initio points. DMBE II and DMBE III potentials differ in the short-range three-body terms used.[17] While DMBE II parameters representing the short-range potential were obtained as a fit to ab initio data, the DMBE III parameters were obtained to reproduce spectroscopic force fields of HO_2. The DMBE IV PES of Pastrana et al. is a further improvement of the DMBE III PES and includes additional ab initio data.[19] The additional ab initio data treat the region of the HO_2 potential, referred to as the H atom exchange region. Large basis sets and correlated multireference wave functions were used in these calculations. The ab initio potential energy was calculated for two different doublet states ($^2B_1$ and $^2A_2$) of HO_2. The $^2B_1$ state is repulsive and corresponds to the ground state of $H + O_2$ products, while the $^2A_2$ has an attractive interaction and correlates with the excited state of O_2. The DMBE IV surface was one of the first global potential surfaces for the $H + O_2 \leftrightarrow HO_2 \leftrightarrow OH + O$ reaction. It is a fit not only to ab initio quantum chemical calculations collected from three sources[18−20] but also a fit to an estimate of the depth of the HO_2 potential well and to the quadratic force field for the HO_2 radical.

After the DMBE IV surface was developed, more extensive and more accurate ab initio calculations for the HO_2 system became available; observations[21] that the DMBE IV surface did not adequately fit these later ab initio results very well motivated the development of other potential surfaces for the $H + O_2 \leftrightarrow HO_2 \leftrightarrow OH + O$ reaction. Kendrick and Pack,[22] for example, used a diatomics-in-molecules approach to fit the ab initio calculations of Walch and co-workers,[21] with particular emphasis on understanding the shape of the PES near the conical intersections of the HO_2 system.

More recently, Troe and Ushakov[23] (TU) developed a global PES for the $H + O_2 \leftrightarrow HO_2 \leftrightarrow OH + O$ reaction based on a set of ab initio calculations by Harding and co-workers.[24,25] These ab initio calculations used the augmented, correlation-consistent polarized triple-ζ (aug-cc-pvtz) basis set of Dunning and co-workers.[26−28] The calculations used the multireference configuration interaction method. In these ab initio calculations, the orbitals were optimized in a state-averaged MCSCF calculation by equally weighting the six doublet states that correlate with the products, $OH(^2P) + O(^3P)$. While the DMBE IV PES provides a satisfactory global PES for the HO_2 system, the ab initio data for the TU PES focuses on the region of the minimum energy paths for the $HO + O$ and $H + O_2$ approaches. In order to obtain a global PES, the ab initio data calculated for the $H + O_2$ and $HO + O$ sides have been combined using a switching technique. As we point out in more detail below, the barrier for H atom transfer in reaction 2b is substantially lower for the TU surface than for the DMBE IV surface. In this regard, it is interesting to note that Varandas found a very low probability for reaction 2b in QCT simulations employing the DMBE IV PES.[12]

TABLE 1: Equilibrium Geometries, Energies, and Vibrational Energies on the DMBE IV and TU Potential Energy Surfaces[a,b]

	$H + O_2$	HO_2	$OH + O$
	DMBE IV PES		
r_{OH}		1.83	1.83
r_{OO}	2.28	2.51	
α		104.3	
energy	−13.4	−68.2	0.00
	TU PES		
r_{OH}		1.88	1.85
r_{OO}	2.54	2.57	
α		100.1	
energy	−13.6	−60.7	0.0

[a] Distances are measured in au and angles in deg. [b] Energies are reported in kcal/mol relative to the OH + O asymptote.

TABLE 2: Internal Energy of OH and O_2 as a Function of the Vibrational Level, for $j = 0$[a]

quantum no.	DMBE IV OH	TU OH	exptl OH[b]	DMBE IV O_2	TU O_2	exptl O_2[c]
4	43.4	43.9	43.1	19.6	19.5	19.6
5	51.7	51.9	51.4	23.8	23.6	23.8
6	59.5	59.7	59.3	28.0	27.6	28.0
7	66.8	66.5	67.1	32.1	31.6	32.0
8	73.6	72.8	74.1	36.1	35.4	36.0
10				43.9	42.8	43.8
15				62.2	59.9	62.1
20				78.4	74.9	78.8

[a] Energies are reported in kcal/mol. [b] Ref 41. [c] Refs 42−47.

Both the DMBE IV and TU PESs have been used in a number of theoretical studies of the OH + O reaction.[12,23] There has so far been no direct comparison of the results obtained by using these two PESs. In this work, we use both the DMBE IV and TU potential surfaces to compute initial-state-specific OH* quenching probabilities for OH* + O collisions; our ultimate goal is a better understanding of how changes in the topography of the underlying PES affect the dynamics of OH* + O collisions and the subsequent quenching of OH* by atomic oxygen. Here we present results for central (zero impact parameter) collisions with zero total angular momentum and a relative translational energy of 0.6 kcal/mol, which corresponds to the average center-of-mass collision energy at $T = 200$ K, a temperature representative of the terrestrial mesosphere. By doing so, we focus our attention on the role of the OH* vibrational energy in the reaction dynamics. The importance of reagent vibrational excitation in simple A + BC systems has long been a subject of considerable interest.[29−40] Studies of the OH* + O reaction not only provide further insight into this subject but might also provide kinetic data that could improve current models of the mesospheric energy balance.

Computational Details

Potential Energy Surfaces. Two PESs are used in the current study. The DMBE IV PES, as noted above, was fit to ab initio calculations collected from three sources as well as the HO_2 well depth and force field. The TU PES was also fit to a set of ab initio calculations largely concentrated in the vicinity of the minimum energy path for the reaction $H + O_2 \rightarrow OH + O$.

Table 1 shows some key characteristics of the two potential surfaces. The two surfaces give very similar exothermicities for the process $OH + O \rightarrow H + O_2$ (reaction 2a). The stable HO_2

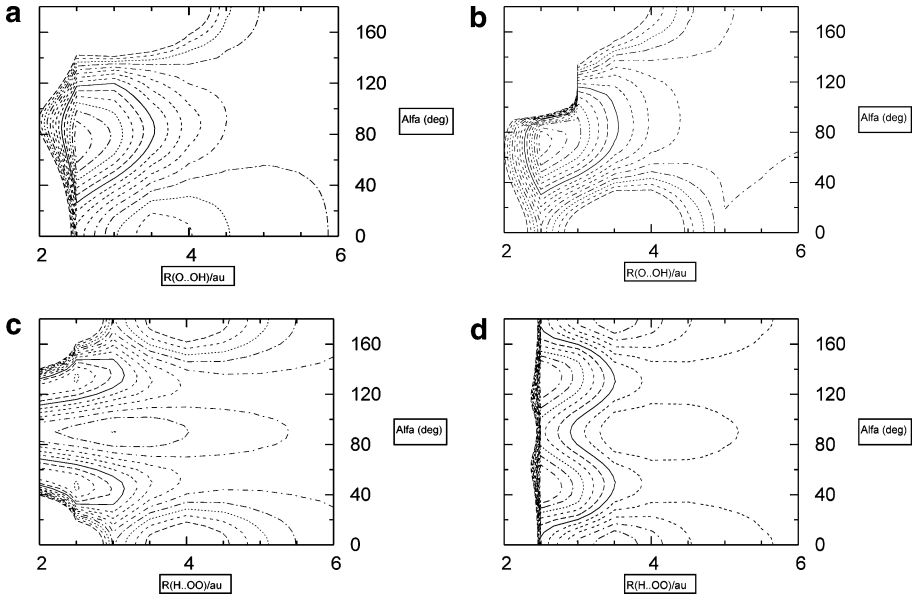

Figure 1. (a) Contour plot of the DMBE IV PES as a function of R(O···OH), the distance of an O atom from the center of mass of OH (in au), and α, the angle (in deg) between the OH and the line joining the O atom and the center of mass of OH. The contours are shown at intervals of 0.01 au with the lowest contour at −0.27 au. The OH is fixed at its equilibrium bond length of 1.83 au. (b) Contour plot of the TU PES as a function of R(O···OH), the distance of an O atom from the center of mass of OH (in au), and α, the angle (in deg) between the OH and the line joining the O atom and the center of mass of OH. The contours are shown at intervals of 0.01 au with the lowest contour at −0.27 au. The OH is fixed at its equilibrium bond length of 1.85 au. (c) Contour plot of the DMBE IV PES as a function of R(H···OO), the distance of an H atom from the center of mass of O_2 (in au), and α, the angle (in deg) between O_2 and the line joining the H atom and the center of mass of O_2. The contours are shown at intervals of 0.01 au with the lowest contour at −0.27 au. The O_2 is fixed at its equilibrium bond length of 2.28 au. (d) Contour plot of the TU PES as a function of R(H···OO), the distance of an H atom from the center of mass of O_2 (in au), and α, the angle (in deg) between O_2 and the line joining the H atom and the center of mass of O_2. The contours are shown at intervals of 0.01 au with the lowest contour at −0.27 au. The O_2 is fixed at its equilibrium bond length of 2.54 au.

radical is the minimum energy configuration for both surfaces. The DMBE IV surface predicts this configuration to be 7.5 kcal/mol more stable than does the TU surface. The equilibrium geometry of the HO_2 radical is roughly the same for the two surfaces, although the OH and OO bonds of this radical are each about 0.05 au longer for the TU PES. One substantial difference between the two surfaces is in the equilibrium bond length of the O_2 product of reaction 2a; the DMBE IV PES gives an O_2 equilibrium bond length of 2.28 au, in good agreement with experiment, while the TU PES gives an O_2 equilibrium bond length of 2.54 au. We note that the switching function used in the TU PES uses a value for r_e of 2.54 au in the Morse potential for the O_2 diatomic.

Table 2 presents the energies of selected OH and O_2 vibrational levels computed from the two surfaces. These energies were calculated by computing the classical vibrational action, as described below in further detail. The experimentally measured energies are also shown for comparison. The vibrational energies of the OH reagent are nearly the same for both surfaces and agree well with experimental data. The vibrational energies of O_2 calculated on the two surfaces are also in good agreement with each other and with experiment for low vibrational levels ($v \leq 6$). For higher vibrational levels, the vibrational energy predicted by the TU PES is lower than that calculated on the DMBE IV PES and the experimental results.

Figures 1−4 depict the overall topography of the two surfaces. In Figure 1, parts a and b, the potential contours are plotted as a function of the Jacobi coordinates, R_{O-OH} and α_{O-OH}, for the DMBE IV and the TU PESs. R_{O-OH} is the distance of the O atom from the center of mass of OH, and α_{O-OH} is the angle between the axis of OH and the line joining the center of mass of OH and the O atom. The O−H bond distance is fixed at its equilibrium value on both surfaces. The TU PES exhibits a repulsive ridge, particularly for large values of the angle α_{O-OH}, which correspond to the O atom approaching from the O end of the hydroxyl radical. The geometries and energies of the complex are similar on the two surfaces. In Figure 1, parts c and d, a similar Jacobi plot is shown as a function of the distance, R_{H-OO}, and the angle, α_{O-OH}, of the H atom with respect to the diatomic oxygen molecule. The O−O bond distance in the oxygen molecule is fixed at its equilibrium value. The two symmetrically located potential wells correspond to the OOH complex on both surfaces. The TU PES exhibits a repulsive ridge for values of R_{H-OO} less than 2.5 au.

The potential energy barriers for the H atom exchange between these two complex geometries are different on the two potential energy surfaces. The saddle point geometry for the H atom exchange reaction is expected to have C_{2v} symmetry. We have, therefore, graphed the potential energy of the HO_2 species in the C_{2v} geometry as a function of the distance of the H atom from the O_2 center of mass (R_{H-OO}) in Figure 2a. The potential energy for each value of R_{H-OO} corresponds to the optimal value of the O−O bond distance. The major difference between the two PESs appears to be for the saddle point geometries for R_{H-OO} distances below 3.5 au. While the energy predicted by the TU PES is lower for R_{H-OO} values up to about 2.2 au, the saddle point energy also rises very steeply on this PES for R_{H-OO} values smaller than 2.5 au. The saddle point energies are larger on the DMBE IV PES, but the increase in energy is observed only for R_{H-OO} values smaller than about 1.8 au, and the increase is not as steep as for the TU PES.

Figure 2b shows the barrier for H atom exchange between these two potential wells, on the two different potential energy surfaces, as a function of the O−O bond distance. The barrier heights for H atom exchange are calculated as the difference between the saddle point energy and the energy corresponding to the complex, for fixed O−O bond length. As seen from the figure, for large values of the O−O bond distance, the barrier

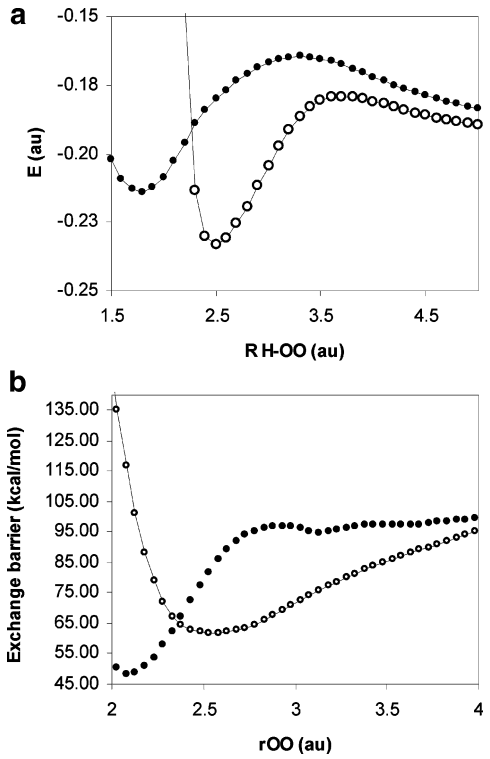

Figure 2. (a) Potential energy of O_2 + H at the C_{2v} geometry on the DMBE IV (●) and TU PES (○) as a function of the H−O_2 center-of-mass distance. For fixed values of the H−O_2 distance, the potential energy is plotted for the optimal value of the O−O bond distance. (b) Barrier for exchange of an H atom on the DMBE IV (●) and TU PES (○) as a function of the O−O bond distance. For each value of the O−O bond length, the maximum and minimum potential energy values are found by searching the grid of potential energy values for 2 au ≤ R_{H-OO} ≤5 au and 40° ≤ α_{H-OO} ≤ 120°. R_{H-OO} is the distance between the H atom and the center of mass of O_2, and α_{H-OO} is the angle between O−O bond and R_{H-OO}.

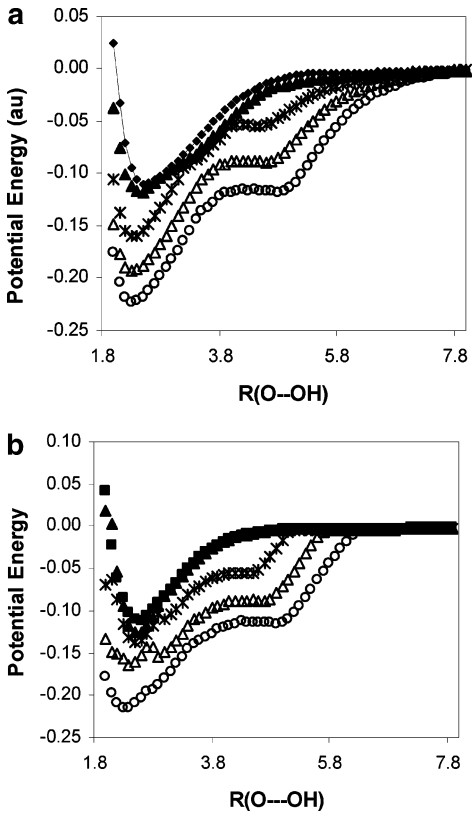

Figure 3. (a) Potential energy as a function of R_{O-OH}, the distance of the O atom from the center of mass of OH, on the DMBE IV PES. The OH bond is held at the outer turning point associated with the vibrational level $v = 0$ (■), 2 (▲), 4 (×), 6 (△), and 8 (○). The angle, α_{O-OH}, between R_{O-OH} and the O−H bond is optimized for each value of R_{O-OH}. (b) Potential energy as a function of R_{O-OH}, the distance of the O atom from the center of mass of OH, on the TU PES. The OH bond is held at the outer turning point associated with the vibrational level $v = 0$ (■), 2 (▲),4 (×), 6 (△), and 8 (○). The angle, α_{O-OH}, between R_{O-OH} and the O−H bond is optimized for each value of R_{O-OH}.

heights for the two surfaces are comparable in magnitude. However, for O−O bond distances smaller than about 3.5 au, the barrier on the TU PES decreases with decreasing distance, reaching a minimum barrier of about 62 kcal/mol at an O−O distance closer to the equilibrium geometry of O_2. By comparison, on the DMBE IV PES, the barrier increases with decreasing O−O distance and reaches a maximum of about 97 kcal/mol, at a O−O distance of about 2.93 au, and then decreases with decreasing distance, reaching a minimum barrier height of about 48 kcal/mol. For O−O distances between 3.5 and 2.4 au, TU PES predicts a substantially smaller barrier for H atom exchange. The difference in the location of the minimum in the exchange barrier on the two surfaces is probably a consequence of the very different O−O equilibrium bond lengths predicted on these surfaces. If the calculated results on the TU PES are translated so that the location of the minima match on the two surfaces, we still find that the exchange barriers predicted by TU PES are smaller than that for the DMBE IV PES for O−O distances greater than that at the minimum, while the opposite is true for O−O distances smaller than that at the minimum.

In Figure 3, we show the potential energy corresponding to the minimum energy path for the approach of the O atom to the OH radical for the different vibrational states of OH considered in this study. The O−H bond distance is held constant at the outer classical turning point for a given OH* level. The optimum approach angle is determined for the various atom−diatom distances. At low translational energies, it is probable that the OH radical will reorient itself to the approaching O atom in order to follow the minimum energy pathway. The well depth, corresponding to the formation of the HO_2 complex, calculated relative to the OH(v) + O asymptote, increases with increasing vibrational state of the OH on both surfaces. The potential energy of the complex, however, increases from $v = 0$ to $v = 2$ and then decreases with increasing vibrational quantum number. The variations of well depths predicted by TU and DMBE IV PES are in qualitative and quantitative agreement. For $v = 0-2$, the shapes of the curves and the well depth are almost the same. Beginning with the $v = 3$ level, the potential energy decreases very sharply at large distances, reaches a plateau, and then decreases more slowly until the minimum corresponding to the complex is reached. There is also a substantial increase in the well depth between $v = 0-2$ and $v \geq 3$ for DMBE IV PES and $v \geq 4$ for TU PES.

In Figure 4, the potential contours are plotted as a function of the O−O and O−H bond distances for two different OOH angles. Figure 4a corresponds to the DMBE IV PES for OOH angle equal to 104.3°, and Figure 4b is for the TU PES for an OOH angle of 100.1°. These OOH angles correspond to the equilibrium geometry of the HO_2 complex on the two surfaces. The TU PES exhibits a very small barrier in the exit channel around an O−H bond distance of 4 au, while no such barrier is found in the exit channel on the DMBE IV PES. The repulsive wall around the complex geometry is again different on the two surfaces. Parts c and d of Figure 4 are corresponding figures

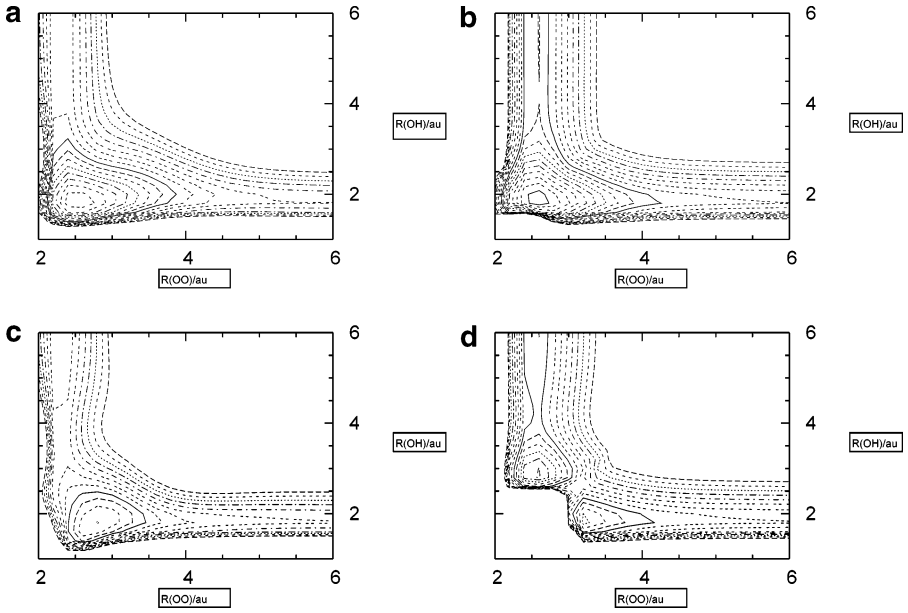

Figure 4. (a) Contour plot of the DMBE IV PES as a function of the O−O distance (*X*-axis, au) and the O−H distance (*Y*-axis, au) for an OOH angle of 104°. The contours are shown at intervals of 0.01 au with the lowest contour at −0.27 au. (b) Contour plot of the TU PES as a function of the O−O distance (*X*-axis, au) and the O−H distance (*Y*-axis, au) for an OOH angle of 100°. The contours are shown at intervals of 0.01 au with the lowest contour at −0.27 au. (c) Contour plot of the DMBE IV PES as a function of the O−O distance (*X*-axis, au) and the O−H distance (*Y*-axis, au) for an OOH angle of 60°. The contours are shown at intervals of 0.01 au with the lowest contour at −0.23 au. (d) Contour plot of the TU PES as a function of the O−O distance (*X*-axis, au) and the O−H distance (*Y*-axis, au) for an OOH angle of 60°. The contours are shown at intervals of 0.01 au with the lowest contour at −0.23 au.

TABLE 3: Scattering Probabilities as a Function of OH Vibrational Quantum Number

reaction type	$v = 1$	$v = 2$	$v = 3$	$v = 4$	$v = 5$	$v = 6$	$v = 7$	$v = 8$
				DMBE IV				
reaction	0.178 ± 0.003	0.360 ± 0.003	0.448 ± 0.004	0.452 ± 0.003	0.403 ± 0.003	0.438 ± 0.003	0.468 ± 0.003	0.645 ± 0.003
exchange	0.169 ± 0.003	0.168 ± 0.003	0.190 ± 0.003	0.173 ± 0.003	0.193 ± 0.003	0.192 ± 0.003	0.152 ± 0.002	0.129 ± 0.002
inelastic	0.653 ± 0.003	0.473 ± 0.003	0.361 ± 0.003	0.375 ± 0.003	0.404 ± 0.003	0.370 ± 0.003	0.381 ± 0.003	0.227 ± 0.003
total removal probability	0.674	0.744	0.895	0.933	0.899	0.945	0.924	0.959
				TU				
reaction	0.516 ± 0.003	0.498 ± 0.003	0.513 ± 0.004	0.471 ± 0.003	0.444 ± 0.003	0.376 ± 0.003	0.491 ± 0.004	0.487 ± 0.004
exchange	0.036 ± 0.001	0.026 ± 0.001	0.051 ± 0.002	0.179 ± 0.003	0.203 ± 0.003	0.262 ± 0.003	0.204 ± 0.003	0.226 ± 0.003
inelastic	0.447 ± 0.003	0.475 ± 0.003	0.435 ± 0.003	0.350 ± 0.003	0.353 ± 0.003	0.362 ± 0.003	0.305 ± 0.003	0.287 ± 0.003
total removal probability	0.777	0.828	0.810	0.819	0.803	0.739	0.831	0.858

for an OOH angle of 60° on DMBE IV and TU PES, respectively. These figures are representative of contours for OOH angles smaller than for the equilibrium geometry of the complex. On the TU PES, approach of the O atom at small angles encounters a rather large repulsive wall even at O−O distances greater than 3 au. On the DMBE IV PES, a similar approach of the O atom does not encounter such a repulsive wall, though there is now a small barrier in the exit channel.

Dynamics. Classical analogues of the quantized (v, j) rovibrational levels of OH and O_2 molecules are defined prior to our QCT simulations using the following procedure. For each vibrational and rotational quantum state of the diatomic species, an initial guess is made for the coordinates of the atoms at the inner turning point. The equations of motion are integrated, and the radial momentum vector, P_r, and the radial coordinate, r, are stored as a function of time. The time integration is continued until the radial momentum changes sign (at the outer turning point). The value of the integral, $\int P_r\, dr$, between the inner and outer turning points is then calculated and compared to the action variable, $(v + 0.5)\pi$. If the relative error between these quantities is greater than 1×10^{-3}, the initial guess for the inner turning point is changed and the calculation repeated until the calculated value for $\int P_r\, dr$ equals $(v + 0.5)\pi$ to within the allowed error. The converged results for the inner and outer turning points, vibrational period, and the total energy of the diatomic molecule, $E(v, j)$, are then stored as a function of the vibrational (v) and rotational (j) quantum states. These calculations are carried out for OH and O_2 on both potential surfaces used in this study. The results obtained are compared with experimental data in Table 2. Note that our definition of the classical (v, j) analogues omits consideration of either the OH electronic orbital angular momentum or the quantum statistical effects associated with the homonuclear character of O_2.

For a given initial (v, j) state of the OH* reactant, a batch of classical trajectories is prepared. Each trajectory in the batch has the same value of the impact parameter b ($b = 0$ unless otherwise specified) and relative translational energy (0.6 kcal/mol). The OH* reagent has rotational quantum number $j = 0$ for each batch of trajectories. The trajectories are initiated with the O atom 10 au from the OH center of mass. The initial OH* conditions for a given trajectory are obtained by starting the OH molecule at its inner classical turning point and propagating it forward in time for a time interval randomly chosen to lie between zero and the classical vibrational period of the OH*

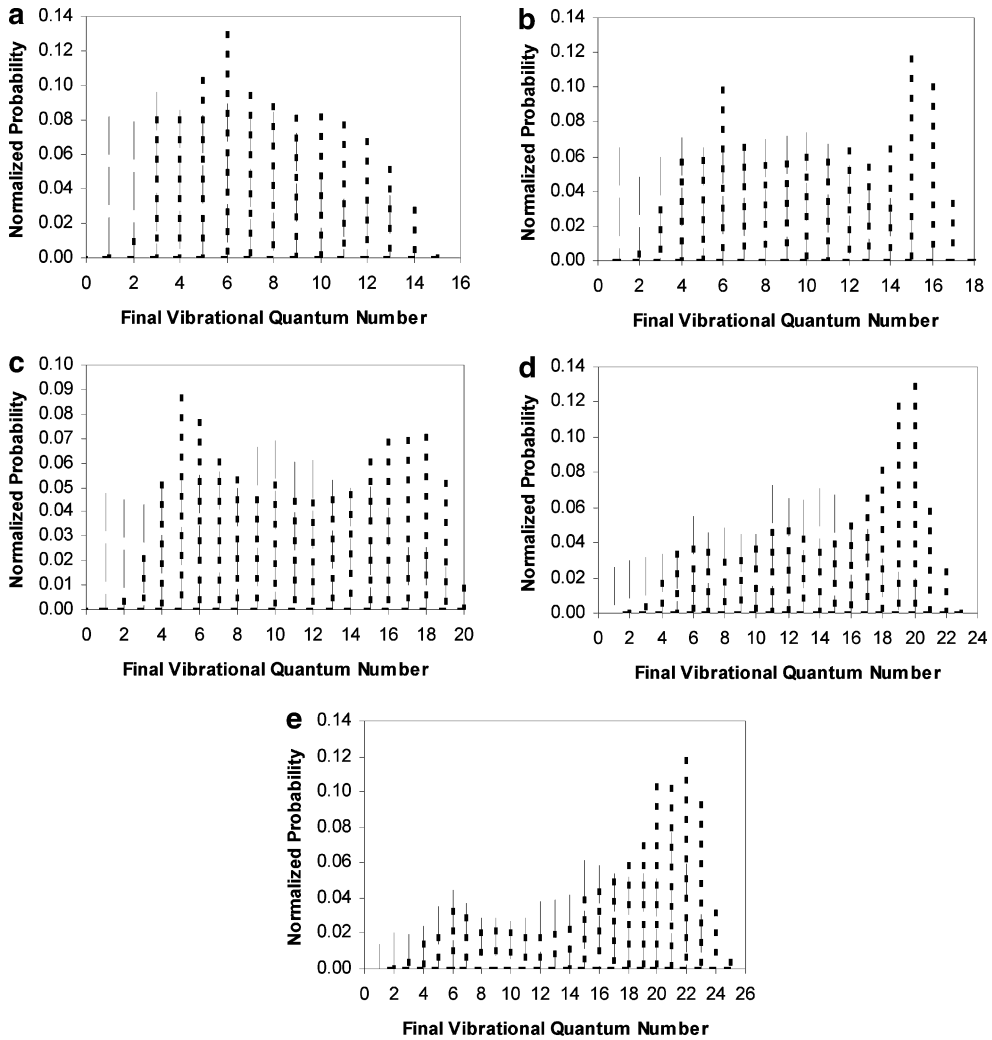

Figure 5. (a) Vibrational state distribution of the O_2 product calculated on the DMBE IV (− − −) and TU (- - -) PES. The initial $v_{OH} = 4$. The length of each bar represents the magnitude of the normalized exchange probability. (b) Vibrational state distribution of the O_2 product calculated on the DMBE IV (− − −) and TU (- - -) PES. The initial $v_{OH} = 5$. The length of each bar represents the magnitude of the normalized exchange probability. (c) Vibrational state distribution of the O_2 product calculated on the DMBE IV (− − −) and TU (- - -) PES. The initial $v_{OH} = 6$. The length of each bar represents the magnitude of the normalized exchange probability. (d) Vibrational state distribution of the O_2 product calculated on the DMBE IV (− − −) and TU (- - -) PES. The initial $v_{OH} = 7$. The length of each bar represents the magnitude of the normalized exchange probability. (e) Vibrational state distribution of the O_2 product calculated on the DMBE IV (− − −) and TU (- - -) PES. The initial $v_{OH} = 8$. The length of each bar represents the magnitude of the normalized exchange probability.

reagent's initial (v, j) state. The orientation of the OH* reagent is then chosen randomly; as the initial OH* state has $j = 0$, no randomization of the OH* angular momentum vector is needed. The equations of motion defining the trajectory are integrated using a fourth-order Runge−Kutta method. An integration step size of 1.2×10^{-17} s is used. Integration accuracy is checked by conservation of energy and momenta and by back-integration. Total energy, total angular momentum, and total linear momentum components are conserved to one part in 10^{-8}.

The diatomic distances are inspected periodically, and the product AB is assumed to be formed if all three of the following criteria are met:

$$r_{AB} < r_{BC} \quad \text{and} \quad r_{AB} < r_{AC}; \quad r_{BC} \quad \text{and} \quad r_{AC} > 15 \text{ au} \tag{3}$$

The angle between $\mathbf{R}_{\mathbf{C-AB}}$, the distance vector of C to the center of AB, and $\mathbf{P}_{\mathbf{C}}$, the momentum vector of C, corresponds to C moving away from AB:

$$E = E_{kin} - (V_{tot} - V_{AB+C}) > 0 \tag{4}$$

TABLE 4: Fraction of Total Available Energy Present as Product Vibration[a]

v_{OH}	$v(O_2)^{mp}$	$E_{int}(O_2)(v^{mp}, j = 0)$	% available energy
		DMB E IV	
4	3	15.4	27
5	10	43.9	67
6	10	43.9	60
7	14	58.7	73
8	21	81.4	93
		TU	
4	10	42.8	74
5	15	59.9	91
6	18	69.2	94
7	20	74.9	94
8	22	79.6	91

[a] $v(O_2)^{mp}$ is the most probable vibrational level of the product. The internal energy of O_2 is calculated corresponding to this vibrational level and a rotational level of 0.

where E_{kin} is the relative kinetic energy, V_{tot} is the total potential energy, and V_{AB+C} is the potential energy of the products. The

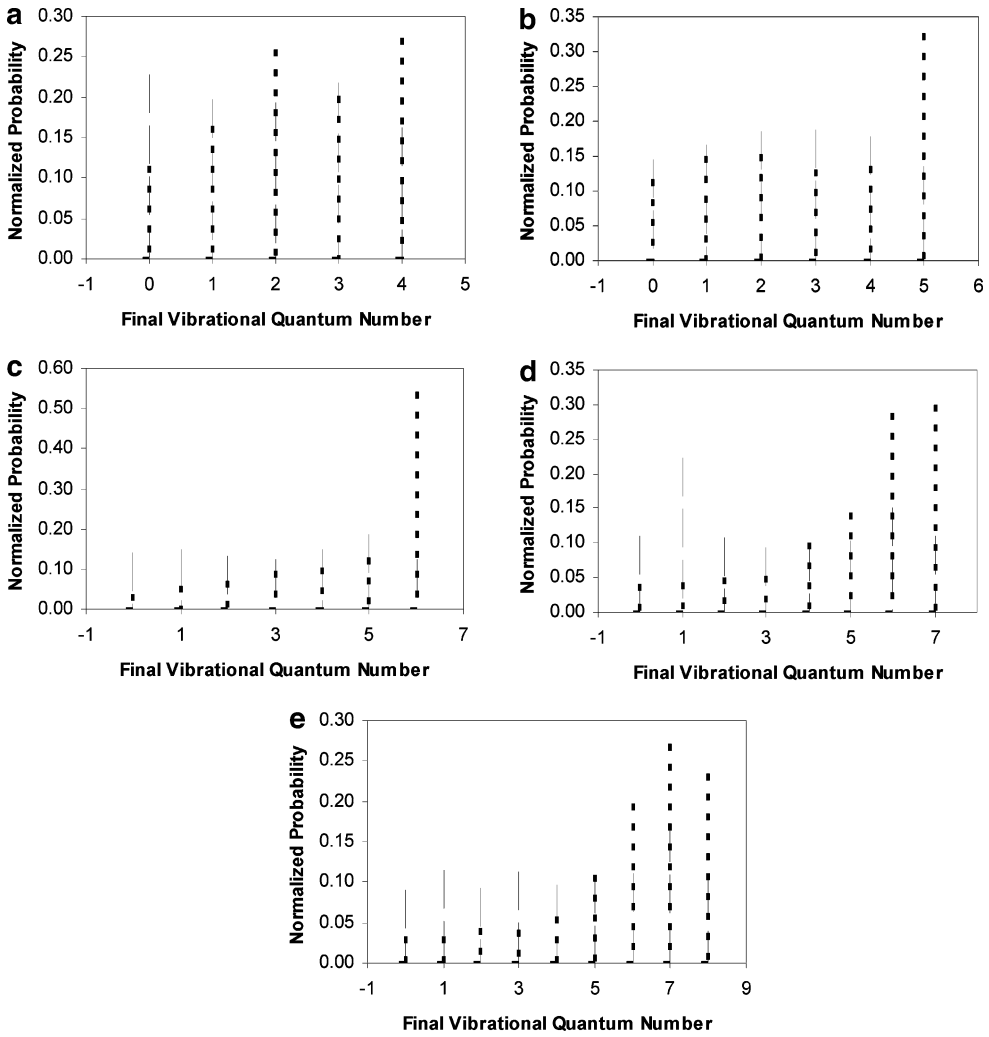

Figure 6. (a) Vibrational state distribution of the exchange product, O^2H, calculated on the DMBE IV (− − −) and TU (- - -) PES. The initial $v_{OH} = 4$. The length of each bar represents the magnitude of the normalized exchange probability. (b) Vibrational state distribution of the exchange product, O^2H, calculated on the DMBE IV (− − −) and TU (- - -) PES. The initial $v_{OH} = 5$. The length of each bar represents the magnitude of the normalized exchange probability. (c) Vibrational state distribution of the exchange product, O^2H, calculated on the DMBE IV (− − −) and TU (- - -) PES. The initial $v_{OH} = 6$. The length of each bar represents the magnitude of the normalized exchange probability. (d) Vibrational state distribution of the exchange product, O^2H, calculated on the DMBE IV (− − −) and TU (- - -) PES. The length of each bar represents the magnitude of the normalized exchange probability. (e) Vibrational state distribution of the exchange product, O^2H, calculated on the DMBE IV (− − −) and TU (- - -) PES. The length of each bar represents the magnitude of the normalized exchange probability.

final rotational quantum number of the diatomic product is calculated using the following:

$$j_{AB} = \text{int}(-0.5 + 0.5\ \text{sqrt}(1.0 + 4.0L_{AB}^2)) \quad (5)$$

where L_{AB}^2 is the square of the total rotational angular momentum of the AB molecule. Knowing the final total internal energy, E_{int}, of the product diatomic molecule, and the rotational quantum number, j_{AB}, the $E(v, j)$ grid of internal energies (previously calculated and stored for each diatomic species) is searched to determine the value for the final vibrational quantum number, v_{AB}. v_{AB} is defined as the value of v for which $|E_{int} - E(v, j_{AB})|$ is a minimum.

State-specific reaction and quenching probabilities are calculated for reactions 2a−2c as follows. We consider a batch of N_{tot} trajectories for which the initial OH* rovibrational state is $(v, j = 0)$. If $N(AB, v', j')$ is the number of trajectories in the batch that form the AB product in the final rovibrational state (v', j'), we define $N(AB, v')$ as

$$N(AB, v') = \text{sum over all } j'\ N(AB, v', j') \quad (6)$$

The probability that OH* reagents in the initial vibrational state v produce AB products in vibrational state v' is then

$$P_v(AB, v') = N(AB, v')/N_{tot} \quad (7)$$

The 68% confidence limit interval for $P_v(AB, v')$ is computed according to

$$\Delta P = [N - N(AB, v')/N_{tot}\,N(AB, v')]^{1/2} P_v(AB, v') \quad (8)$$

Results and Discussion

Our calculated probabilities for the scattering events 2a, 2b, and 2c on the two potential surfaces are given in Table 3, as a function of v, the initial vibrational state of OH. Each value in the table is the result of an ensemble of 20 000 trajectories. The error bars represent the 68% confidence interval. The probability of reactive scattering for these central collisions is larger than that for exchange by a factor of 2−3 on the DBME IV PES for $v = 2$−7. The ratio of the probability for reaction to exchange reaches a minimum value of 2.09 for $v = 5$, then increases to almost 5 for $v = 8$. The probability for reaction is

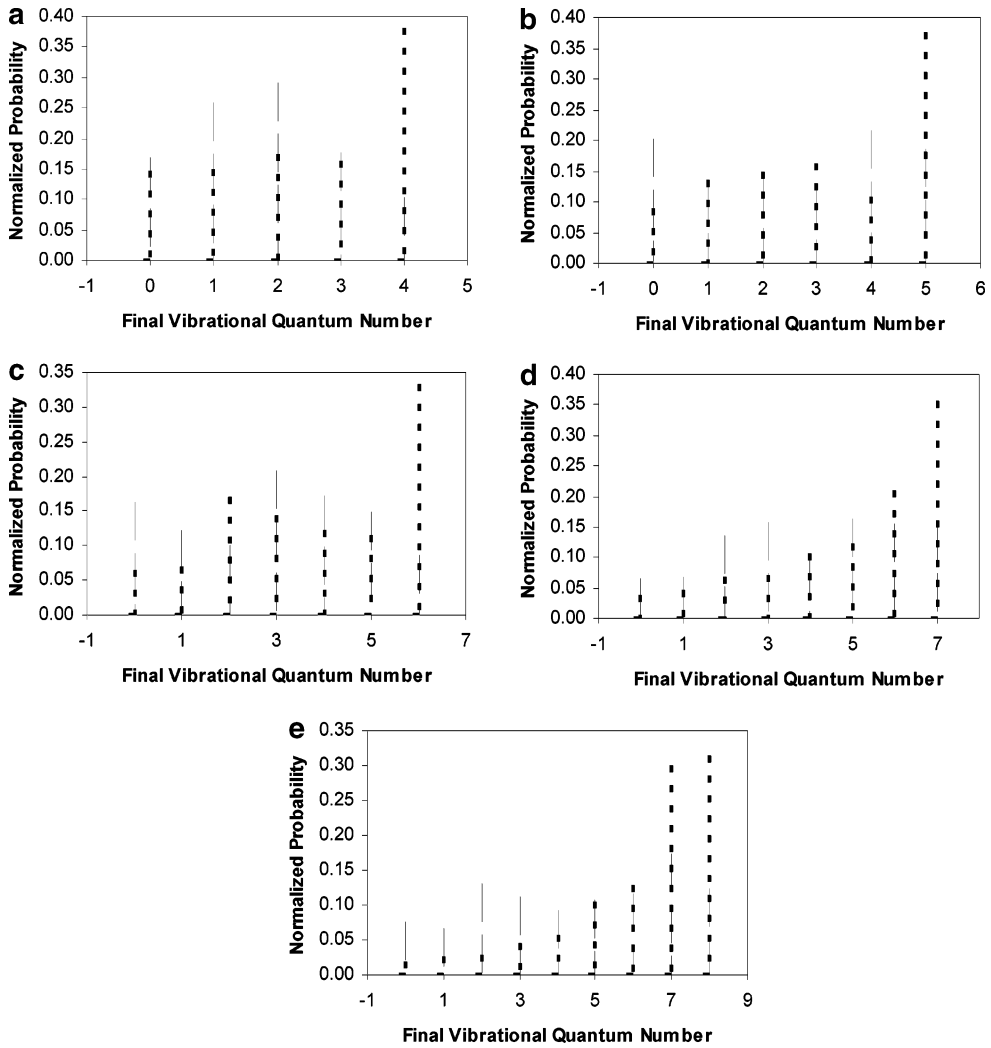

Figure 7. (a) Vibrational state distribution of the inelastic product, O^1H, calculated on the DMBE IV (− − −) and TU (- - -) PES. The initial $\nu_{OH} = 4$. The length of each bar represents the magnitude of the normalized inelastic probability. (b) Vibrational state distribution of the inelastic product, O^1H, calculated on the DMBE IV (− − −) and TU (- - -) PES. The initial $\nu_{OH} = 5$. The length of each bar represents the magnitude of the normalized inelastic probability. (c) Vibrational state distribution of the inelastic product, O^1H, calculated on the DMBE IV (− − −) and TU (- - -) PES. The initial $\nu_{OH} = 6$. The length of each bar represents the magnitude of the normalized inelastic probability. (d) Vibrational state distribution of the inelastic product, O^1H, calculated on the DMBE IV (− − −) and TU (- - -) PES. The initial $\nu_{OH} = 7$. The length of each bar represents the magnitude of the normalized inelastic probability. (e) Vibrational state distribution of the inelastic product, O^1H, calculated on the DMBE IV (− − −) and TU (- - -) PES. The initial $\nu_{OH} = 8$. The length of each bar represents the magnitude of the normalized inelastic probability.

greater than that for exchange on the TU PES as well. This ratio, however, is not as strongly dependent on ν as on the DMBE IV PES, for $4 \leq \nu \leq 8$. The reaction to exchange probability ratio increases with decreasing ν and is almost 20 for $\nu = 2$; for other vibrational levels this ratio is between 2 and 3. Thus, the exchange probabilities at low values of ν are significantly smaller on the TU PES than the DMBE IV PES.

The probability for reaction on the two surfaces is between 40% and 50% for $\nu = 3-7$; it appears to reach a plateau on the TU PES around $\nu = 4$ with minor oscillations, while on the DMBE IV PES, for $\nu = 8$, a much larger reaction probability is observed. This feature can be attributed to the highly repulsive wall encountered on the TU PES for small OH bond distances. From Figure 4, parts b and d, we see that as the O atom approaches the OH closer to its inner turning point, it encounters a strong repulsive potential on the TU PES. The repulsive wall is even stronger for smaller OOH approach angles (Figure 4d). For higher vibrational levels of OH, there is a greater probability of trajectories encountering the repulsive wall, and such trajectories are less likely to lead to reaction on the TU PES compared to the DMBE IV PES. For $\nu_{OH} \leq 3$, the reaction probabilities remain high on the TU PES, while it decreases to about 20% for $\nu = 1$ on the DMBE IV PES. This could be attributed to the very similar O−O equilibrium bond lengths for O_2 and the HO_2 complex on the TU PES. Hence, it will be very easy for the HO_2 complex to dissociate to the vibrational ground state of O_2. On the DMBE IV PES, however, due to the mismatch of the O−O equilibrium bond distances in O_2 and HO_2, the O_2 molecule will probably have to be formed in an excited vibrational state. Vibrational energy generally tends to remain vibrational energy rather than be transformed to rotational or relative translational energy. Thus, vibrational excitation of OH has a significant effect on the reaction probability on the DMBE IV PES, while such an effect is not observed on the TU PES.

The results reported by Varandas[12] using the DMBE IV PES show a similar pattern for the rate coefficients calculated at a temperature of 210 K; however, these rate coefficients cannot be directly compared with the results shown in Table 3. Our trajectories are computed using fixed values for the impact parameter and relative translational energy, whereas the calculations reported by Varandas are averaged over a linear distribu-

tion of impact parameters and are performed at a fixed temperature. It is interesting to note that our results agree qualitatively with the earlier results of Varandas, where different values for the maximum impact parameter were used for each initial vibrational state of OH, ν. The exchange probabilities reported here on the DMBE IV PES reach a maximum value for $\nu = 5$ or 6 and decrease for higher values of ν. The results reported by Varandas for the exchange rate constants also show a similar behavior with a maximum for $\nu = 4$, but for $\nu = 8$, the rate constant is the largest. This is in qualitative disagreement with our results.

In Table 3, we also report the total removal probability which includes the removal of excited OH* by reaction, exchange, or inelastic collisions. The total removal probability on the DMBE IV PES increases with ν, and increases to over 90% for $\nu = 4$. On the TU PES, the total removal probability does not depend as strongly on the vibrational excitation of OH, though a small increase is observed on going from $\nu = 1$ to $\nu = 2$. It is interesting to note that the DMBE IV and TU PES differ considerably in the results for scattering probabilities obtained for low vibrational excitations, $\upsilon \leq 3$. This difference is especially significant, since OH* with $\nu = 1-4$ are expected to be removed primarily by collision with O atoms.

A batch of 20 000 trajectories was also run with an impact parameter of $b = 5$ au and $\nu = 6$ on the DMBE IV PES. The scattering probabilities for reaction, exchange, and inelastic were 0.465, 0.181, and 0.353, respectively. An additional batch of 10 000 trajectories was run for the same initial conditions but averaging over the impact parameter ($b = \xi b_{\max}$, $0 \leq \xi \leq 1$) with a maximum impact parameter of 10.0 au. The reactive, exchange, and inelastic scattering probabilities were 0.457, 0.203, and 0.359, respectively. We note that the scattering probabilities are of similar magnitude for batches of trajectories with $b = 0$, $b = 5$ au, and a linear distribution of b values.

Exchange probabilities are higher on the TU PES for the initial vibrational excitations of OH in the range of $4 \leq \nu \leq 8$. For $\nu < 4$, the exchange probability drops sharply on TU PES, while in this range ν has a negligible effect on exchange probabilities for the DMBE IV PES. As seen from Figure 2, the barrier for exchange is lower on the TU PES for values of the O−O distance between about 3.5 and 2.5 au, and reaches a minimum barrier of about 62 kcal/mol at an O−O distance of 2.5 au. Though the barrier for exchange on the DMBE IV PES is lower by about 20 kcal/mol, this minimum is reached only at an O−O bond distance closer to its equilibrium value of about 2.2 au. At longer O−O bond distances, the exchange barrier is lower on the TU PES. The smaller exchange barrier could account for the larger exchange probabilities observed on this surface, particularly for collisions with $\nu \geq 4$.

In Figure 5a−e we plot the vibrational distribution of the product O_2 molecule for initial vibrational state of OH ranging from $\nu = 4$ to $\nu = 8$, for the DMBE IV and TU PES. The errors in the probability distribution calculated at the 68% confidence interval range from 5% to 8%, except in cases with very low probabilities where the errors are higher. The energy released in the highly exothermic reaction 2a appears predominantly as vibrational energy of the product, O_2, on both surfaces. On the TU PES, on the average, the product molecules are formed with higher vibrational excitation. For example, for the initial vibrational state of $\nu = 7$, the most probable vibrational level of the O_2 diatomic is 20, with an internal energy of 74.9 kcal/mol. This corresponds to about 94% of the total available energy (internal energy of OH, reaction exothermicity, and relative translational energy) appearing as product vibration. A similar result is observed for the other initial vibrational excitations of OH. Table 4 compares the fraction of the total available energy appearing as the vibrational energy of the O_2 molecule for the most probable vibrational state of O_2 on both the PESs. On the TU PES a larger fraction of the total available energy appears as product vibration. The product vibrational distribution, calculated on the TU PES, is bimodal. As the initial vibrational excitation of OH is increased, the bimodality of the distribution is enhanced, and the second peak at the higher vibrational excitation has a much larger probability. For $\nu = 4$, the distribution is very broad and the bimodal behavior has almost disappeared. In each case, the fraction of available energy in product vibration is calculated based on the second peak at the higher vibrational level. The vibrational distribution calculated on the DMBE IV PES exhibits different features. The distribution is rather broad and lacks a bimodal feature. The fraction of total available energy resulting in product vibration is much smaller than on the TU PES.

The vibrational distribution of the exchange product, O^2H, is plotted in Figure 6a−e for the DMBE IV and the TU PES. Here again, the errors in the probability distribution calculated at the 68% confidence interval range from 5% to 6%. The results are significantly different for the two surfaces. The probability of vibrational quenching through an exchange reaction is much smaller on the TU PES for all initial vibrational states investigated. A large fraction of the exchange scattering events is vibrationally adiabatic on this surface. For example, for the initial state $\nu = 6$, greater than 50% of the exchange product is formed in the $\nu' = 6$ state. For initial states $\nu = 7$ and $\nu = 8$, the quenching probability is dominated by $\Delta\nu = 1$. For initial states $\nu = 5$ or 4, there is a slight increase in the multiquantum vibrational transitions. Multiquantum transition probabilities increase with a decrease in the initial vibrational excitation of OH. On the DMBE IV PES, multiquantum vibrational transitions occur for all initial vibrational states of OH with a significant probability. The vibrational distribution of the exchange product on the DMBE IV PES is rather broad, and single-quantum transitions are not the most probable. For both surfaces, the vibrational state distribution of the inelastic product is similar to that for the exchange product, as shown in Figure 7a−e. The TU PES leads predominantly to vibrationally adiabatic inelastic scattering. The DMBE IV PES, on the other hand, leads to inelastic scattering products with multiquantum transitions. Varandas[12] has also observed that multiquantum transitions become less probable with decreasing ν. Similar multiquantum transitions were also observed for the quenching of OH by O_2.[48]

In order to understand the differences in the pathways leading to the three different scattering processes, we examined a large number of trajectories on the two PESs through animations using VMD.[49] A large number of reactive scattering processes on both PESs seem to occur when the O atom approach to the OH radical corresponds to an obtuse OOH angle. For the small number of reactive scattering events that occur when the O atom approach to the OH radical correspond to an acute OOH angles, one or more H atom exchange events occur between the two O atoms, the O−O distance gets closer to the equilibrium bond length and the H atom leaves. Irrespective of the approach angle, the mechanism for reactive scattering appears to be through complex formation, as expected.

On the other hand, inelastic and exchange scattering events occur predominantly for the O atom approach corresponding to acute OOH angles on both PESs. There are rare inelastic scattering events with one or more H atom exchanges. For

inelastic processes associated with an O−O collision, the product OH is highly rotationally excited. On the TU PES, most inelastic processes occur without H atom exchange or O−O collisions.

Exchange scattering processes that occur through multiple H atom exchange events between the two O atoms and are predominantly vibrationally adiabatic. Exchange processes leading to vibrational quenching appear to occur when the O atom approach corresponds to obtuse OOH angles or when there are O−O collisions. On the TU PES, O−O collisions are less favorable owing to the large repulsive interaction at small O−O distances. This should, therefore, make vibrational quenching less likely. Our results showing smaller quenching probabilities for exchange and inelastic scattering processes on the TU PES support this. On the DMBE IV PES, on the other hand, for both exchange and inelastic processes there are one or more collisions between the two O atoms. The higher quenching probabilities on the DMBE IV PES for both these processes could therefore possibly arise from the difference in the O−O short-range potential.

Conclusions

Classical trajectory calculations were used to study the collisional quenching of vibrationally excited OH radicals by O atoms on two different PESs. The reaction probabilities on the two PESs were much larger than exchange and inelastic scattering probabilities. The O_2 product formed is highly vibrationally excited, and a large fraction of the total available energy appears as product vibration. One important difference between the two PESs investigated is the probability of vibrational quenching through exchange or inelastic scattering. These quenching events are much rarer on the TU PES. On the DMBE IV PES, vibrational quenching through multiquantum transitions is found to occur with a significant probability. The mechanism for multiquantum and single-quantum quenching events appears to be the approach of the O atom at close distances to the O atom of the hydroxyl radical. This is accompanied by one or more O−O collisions before product formation. The highly repulsive potential encountered for short O−O distances on the TU PES, especially for certain approach geometries, prevents such close approach of the two O atoms. This decreases the probability of vibrational quenching through exchange or inelastic scattering on this surface.

Acknowledgment. This work was partly supported by the RSEC program funded by the NSF. R. Viswanathan was supported by a summer fellowship by the RSEC program at the University of Tennessee, Knoxville, TN.

References and Notes

(1) Ohoyama, H.; Kasai, T.; Yoshiumura, Y.; Kimura, H.; Kuwata, K. *Chem. Phys. Lett.* **1985**, *118*, 263.
(2) Klenerman, D.; Smith, I. W. M. *J. Chem. Soc., Faraday Trans. 2* **1987**, *83*, 229.
(3) Adler-Golden, S. *J. Geophys. Res.* **1997**, *102*, 19969.
(4) Dyer, M. J.; Knutsen, K.; Copeland, R. A. *J. Chem. Phys.* **1997**, *107*, 7809.
(5) Dodd, J. A.; Lipson, S. J.; Blumberg, W. A. M. *J. Chem. Phys.* **1991**, *95*, 5752.
(6) Chalamala, B. R.; Copeland, R. A. *J. Chem. Phys.* **1993**, *99*, 5807.
(7) Knutsen, K.; Dyer, M. J.; Copeland, R. A. *J. Chem. Phys.* **1993**, *104*, 5798.
(8) Spenceer, J. E.; Glass, G. P. *Int. J. Chem. Kinet.* **1977**, *11*, 97.
(9) Khachatrian, A.; Dagdigian, P. J. *Chem. Phys. Lett.* **2005**, *414*, 1.
(10) Higgins, C.; Ju, Q.; Seiser, N.; Flynn, G. W.; Chapman, S. *J. Phys. Chem. A* **2001**, *105*, 2858.
(11) Frost, R. J.; Smith, I. W. M. *Chem. Phys.* **1987**, *117*, 389.
(12) Varandas, A. J. C. *Chem. Phys. Lett.* **2004**, *396*, 186.
(13) Varandas, A. J. C. *Mol. Phys.* **1984**, *53*, 1303.
(14) Varandas, A. J. C. *THEOCHEM* **1985**, *120*, 401.
(15) Pastrana, M. R.; Quintales, L. A. M.; Brandao, J.; Varandas, A. J. C. *J. Phys. Chem.* **1990**, *94*, 8073.
(16) Varandas, A. J. C.; Brandao, J. *Mol. Phys.* **1986**, *57*, 387.
(17) Varandas, A. J. C.; Brandao, J.; Quintales, L. A. M. *J. Phys. Chem.* **1988**, *92*, 3732.
(18) Melius, C. F.; Blint, R. *J. Chem. Phys. Lett.* **1979**, *64*, 183.
(19) (a) Walch, S. P.; Rohlfing, C. M.; Melius, C. F.; Baushlicher, C. W., Jr. *J. Chem. Phys.* **1988**, *88*, 6273. (b) Walch, S. P.; Rohlfing, C. M. *J. Chem. Phys.* **1989**, *91*, 2373.
(20) Varandas, A. J. C. *J. Chem. Phys.* **1989**, *90*, 4379.
(21) (a) Walch, S. P.; Duchovic, J. R. *J. Chem. Phys.* **1991**, *94*, 7068. (b) Walch, S. P.; Duchovic, J. R. *J. Chem. Phys.* **1992**, *96*, 4050. (c) Walch, S. P.; Rohlfing, C. M.; Melius, C. F.; Bauschilcher *J. Chem. Phys.* **1998**, *88*, 6273.
(22) Kendrick, B.; Pack, R. T. *J. Chem. Phys.* **1995**, *102*, 1994.
(23) Troe, J.; Ushakov, V. G. *J. Chem. Phys.* **2001**, *115* (8), 3621.
(24) Harding, L. B.; Troe, J.; Ushakov, V. G. *Phys. Chem. Chem. Phys.* **2000**, *2*, 631.
(25) Harding, L. B.; Maergoiz, A. I.; Troe, J.; Ushakov, V. G. *J. Chem. Phys.* **2000**, *113* (24), 11019.
(26) Dunning, T. H. *J. Chem. Phys.* **1989**, *90*, 381.
(27) Kendall, R. A.; Dunning, T. H.; Harrison, R. H. *J. Chem. Phys.* **1992**, *96*, 6796.
(28) Woon, D. E.; Dunning, T. H. *J. Chem. Phys.* **1993**, *98*, 1358.
(29) Mlynczak, M. G.; Solomon, J. *Geophys. Res.* **1993**, *98*, 10517.
(30) Mlynczak, M. G.; Zhou, D. K.; Adler-Golden, S. M. *Geophys. Res. Lett.* **1998**, *25*, 647.
(31) Hou, H.; Huang, Y.; Gulding, J.; Rettner, C. T.; Auerbach, D. J.; Wodtke, A. M. *Science* **1999**, *284*, 1647.
(32) Levine, R. D.; Manz, J. *J. Chem. Phys.* **1975**, *63*, 4280.
(33) Ben-Shaul, A.; Levine, R. D.; Bernstein, R. B. *J. Chem. Phys.* **1974**, *61*, 4937.
(34) Procaccia, I.; Levine, R. D. *J. Chem. Phys.* **1975**, *63*, 4261.
(35) Pollak, E.; Levine, R. D. *Chem. Phys. Lett.* **1976**, *39*, 199.
(36) Levine, R. D.; Bernstein, R. B.; Kahana, P.; Procaccia, I.; Upchurch, E. T. *J. Chem. Phys.* **1976**, *64*, 796.
(37) Kaplan, H.; Levine, R. D.; Manz, J. *J. Chem. Phys.* **1976**, *12*, 447.
(38) Oref, I.; Tardy, D. C. *Chem. Rev.* **1990**, *90*, 1407.
(39) Weston, R. E.; Flynn, G. W. *Annu. Rev. Phys. Chem.* **1992**, *43*, 559.
(40) Mullin, A. S., Schatz, G. C., Eds. *Highly Excited Molecules: Relaxation, Reaction and Structure*; American Chemical Society: Washington, DC, 1997.
(41) Dyer, J. M.; Knutsen, K.; Copeland, R. A. *J. Chem. Phys.* **1997**, *107* (19), 7809.
(42) (a) Herzberg, G. *Can. J. Phys.* **1952**, *30*, 185. (b) Broida, H. P.; Gaydon, A. G. *Proc. R. Soc. London* **1954**, *A222*, 181.
(43) Herzberg, G. *Can. J. Phys.* **1953**, *31*, 657.
(44) Babcock, H. D.; Herzberg, L. *Astrophys. J.* **1948**, *108*, 167.
(45) Lochte-Holtgreven, W.; Dieke, G. H. *Ann. Phys.* **1929**, *3*, 937.
(46) Feast, M. W. *Proc. Phys. Soc., London* **1950**, *A63*, 549.
(47) Park, H.; Slanger, T. G. *J. Chem. Phys.* **1993**, *100* (1), 287.
(48) Garrido, J. D.; Caridade, P. J. S. B.; Varandas, A. J. C. *J. Phys. Chem. A* **2002**, *106*, 5314.
(49) Humphrey, W.; Dalke, A.; Schulten, K. *J. Mol. Graphics* **1996**, *14.1*, 33.